

Natural Melanin/Polyurethane Composites as Highly Efficient Near-Infrared-Photoresponsive Shape Memory Implants

Wanjie Xie,[§] Fei Yan,[§] Esfandiar Pakdel, Julie Sharp, Dan Liu, Xungai Wang, Shi Zhan,^{*} and Lu Sun^{*}

Cite This: *ACS Biomater. Sci. Eng.* 2020, 6, 5305–5314

Read Online

ACCESS |

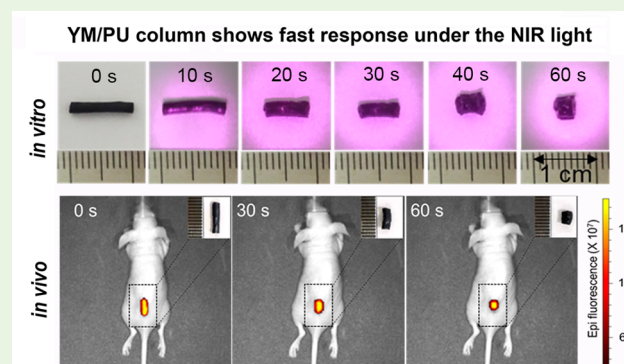
Metrics & More

Article Recommendations

Supporting Information

ABSTRACT: Natural melanin is recognized as a biocompatible photothermal agent because of its biologically derived nature and efficient photothermal conversion ability. Here, yak hair melanin (YM) is added to polyurethane (PU) for the fabrication of NIR-photoresponsive shape memory implants. The *in vitro* toxicity of the YM/PU composites is carried out by exposing them to human mesenchymal stem cells (hMSCs) and mouse fibroblast (L929) cells lines for 24 h, while the *in vivo* toxicity is investigated by implanting the YM/PU composites in the mouse for two months. No significant differences on cell viability, blood chemistry, hematology, and histological results are observed between YM/PU composites and control groups, suggesting their excellent biocompatibility. The biostability of the YM/PU composites is confirmed by monitoring their *in vitro* degradation for 12 weeks. The YM/PU column implanted in the back subcutis or vagina of the mouse rapidly recovered to its original state within 60 s under a very low NIR laser (808 nm, 0.5 W/cm²) intensity, which is much lower than the general laser intensity for photothermal cancer therapy (1–2 W/cm²). This work confirms the applicability of the YM/PU composites as long-term implant materials and expedites the use of YM/PU composites as cost-effective candidates for biomedical applications.

KEYWORDS: natural melanin, near-infrared, photothermal, shape memory, implant



INTRODUCTION

Intelligent shape memory polymers (SMPs) have widely been used in fabricating implantable biomedical devices such as self-expanding stents, intelligent sutures, active catheters, and contraception columns.^{1–4} By fixing these devices into a “temporary” shape and implanting them into the biological systems, they are capable of recovering to a “remembered” permanent shape with the external stimuli such as heat, light, and magnetic field.^{1,5–9} Among various stimuli, near-infrared (NIR) light has attracted the most attention because of its excellent tissue penetration ability and has been widely used in NIR-triggered biomedical systems.^{4,10–12} Using NIR light as the stimulus, photothermal agents can convert the absorbed light energy into heat and are usually added into the SMPs to trigger the shape memory behavior of SMPs.⁷ The most commonly used photothermal agents include gold, carbon, and magnetic nanoparticles, graphene, NIR dyes, or some polymer nanoparticles (i.e., polyaniline, polypyrrole).^{4,13} Despite the extraordinary photothermal effects, the long-term safety issue of these synthetic materials remains as a major concern. For instance, metallic nanoparticles might cause metal-related cytotoxicity in biological systems, and carbon-based nanomaterials can induce oxidative stress and lung inflammation after administration.^{13,14} Furthermore, preparations of these materi-

als require tedious synthetic processes, which are time- and energy-consuming.^{4,15–17} Therefore, it is required to find an alternative material with efficient photothermal conversion efficiency, good price, and easy availability, as well as human-benign nature.

Melanin is a natural pigment that widely appears in animals, plants, and microorganisms.¹⁸ It possesses a series of unique properties and has widely been employed in different applications.^{13,19–29} In particular, it has intrinsic biocompatibility and has been applied as food additives/supplements³⁰ or biocompatible electrode material.^{31,32} It is also considered to be an excellent photothermal agent because of its extremely fast photodynamics, which enable almost complete conversion of the energy of the absorbed photons into heat.³³ In this regard, several studies have successfully applied both synthetic and natural melanin for photothermal therapy.^{13,34–36} Furthermore, NIR-photoresponsive SMPs based on melanin/

Received: June 23, 2020

Accepted: July 28, 2020

Published: July 28, 2020



melanin-like materials have also been developed.^{37–41} However, no SMP-based implantable prototypes have been developed based on melanin, and their long-term toxicity has not been explored. Therefore, it is required to further investigate the related practical applications. More importantly, Jiang et al. previously reported that melanin from cuttlefish ink had much higher photothermal conversion efficiency than PDA, revealing the superiority of natural melanin.¹³ Additionally, natural melanin can be easily derived from some waste materials like hair wastes or squid ink. Therefore, it is a cost-effective candidate to develop NIR-photoresponsive SMP-based implants with fast response.

To this end, we extracted the natural melanin from some textile scraps such as yak hair wastes and explored its applicability for the first time as an effective photothermal agent in developing SMPs implants. The obtained yak melanin (YM) particles were well characterized and then were embedded in polyurethane (PU), followed by demonstrating their NIR-photoresponsive performance. *In vitro* cytotoxicity tests suggested the low toxicity of the YM/PU composites to both human mesenchymal stem cells (hMSCs) and mouse fibroblast cells (L929) cells. The *in vivo* biocompatibility was investigated by implanting the YM/PU composites in the mouse for two months, after which the hematology analysis, blood chemistry analysis and the histological results of the major organs for the tested mouse showed insignificant differences compared with the control groups. The YM/PU composites also showed negligible degradation in the *in vitro* degradation tests for 12 weeks, confirming their biostability and potential to be a long-term implant material. An YM/PU column was fabricated and proposed as a contraception column to be implanted in the fallopian tube. This column was able to recover to its original size *in vivo* within 60 s by using a low NIR laser intensity (808 nm, 0.5 W/cm²). The biostability, biocompatibility, and the fast-responsive performance of the YM/PU composites under NIR light *in vivo* revealed their potential as smart implants.

EXPERIMENTAL SECTION

Materials. Yak hair was provided by the Zhongfuda Textile Co., Ltd. Acetone, sodium phosphate dibasic (Na₂HPO₄), and hydrochloric acid (HCl, 32%) were purchased from Sigma-Aldrich and RCI Labscan Ltd., respectively. Sodium phosphate monobasic dihydrate (NaH₂PO₄·2H₂O) was bought from Fluka Analytical. Dimethyl sulfoxide (DMSO) and polyurethane (PU) pellets (ChronoFLex C 80A) were obtained from Chem-Supply and AdvanSource Biomaterials Corp., respectively. The human mesenchymal stem cells (hMSCs) were provided by CellCare Australia, and mouse fibroblast cells (L929) were obtained from the CellBank Australia. The phosphate buffer solution (PBS, 0.1 M, pH = 7.4) and glutomax were purchased from Gibco, while the fluorescence dye cyanine 5.5 (Cy5.5) was bought from the Abcam Australia Pty Ltd.

Preparation of Yak Melanin. YM was obtained from yak hair as reported in our previous work.^{25,26,42–44} In brief, the yak hair was immersed into acetone for washing, followed by rinsing with deionized water for several times. Afterward, the washed hair was dried in the oven at 60 °C overnight. The isolation process was carried out by immersing the as-prepared yak hair into the HCl solution for 3 h at 100 °C in a three neck round-bottom flask equipped with a condenser. The YM was separated through centrifugation and then washed with distilled water to obtain the neutral supernatant. According to Horvath et al., hair is composed of proteins, lipids, water, and small amounts of trace elements.⁴⁵ In our previous work, it was demonstrated that only the ovoid/spherical melanin particles remained in the solution, indicating that the proteins

and other substances in the hair were removed during the isolation process.⁴³

Preparation of YM/PU Films and YM/PU Column. The YM/PU films were obtained as films by dispersing the YM in DMSO, followed by adding PU pellets with magnetic stirring for 12 h. The YM/PU/DMSO suspensions were then cast on a silicon mold with the evaporation of DMSO in the oven at 90 °C for 12 h. The mass ratio between YM and PU were 0, 0.5, 1, and 2 wt %. A YM/PU column was obtained using a thermoplastic process. In brief, YM/PU films were introduced into a self-made tubular teflon mold (diameter: ~3 mm) and was heated to 220 °C for 30 min. Cy 5.5-labeled YM/PU columns were fabricated by adding Cy5.5 in the YM/PU composites at a mass ratio of 0.1 wt % to the mass of PU.

Characterization. The scanning electron microscopy (SEM) image of YM was obtained using a Zeiss Supra 55 SEM VP microscope (Carl Zeiss, Germany) at the voltage of 5 kV. Transmission electron microscopy (TEM) and high-resolution (HR) TEM images of YM were taken on a JEOL 2100 TEM LaB6 (JEOL, Japan) with a Gatan camera at an accelerating voltage of 200 kV. UV–vis absorption spectra of the YM suspension were obtained on a Cary 300 UV–vis spectrophotometer (300–900 nm). UV–vis absorption spectra of YM/PU films were obtained on a Cary 5000 UV–vis spectrophotometer (300–900 nm). X-ray photoelectron spectroscopy (XPS) spectra of YM were conducted on the AXIS Nova (Kratos Analytical in Manchester, UK). XPS spectra were analyzed on the CasaXPS. The Fourier transform infrared spectroscopy (FTIR) spectra of YM was obtained using a Bruker FTIR spectrophotometer for the YM/KBr pellet with accumulation of 32 scans at 4 cm⁻¹ resolution. Differential scanning calorimetry (DSC) curves of pristine PU and YM-2 wt %/PU films were obtained using a TA Instruments Q200 on an aluminum pan under the nitrogen flow. The temperature was first increased from –80 to 220 °C, then reduced to –80 °C, and again increased to 220 °C. Heating and cooling rate was 5 °C min⁻¹. DSC curves were analyzed by the TA Universal Analysis software to evaluate the shape memory transition temperature (T_{trans}). Water contact angle on the films was determined based on the contact angle measurement system (KSV Instruments Ltd., Finland) and was recorded with a CAM 101 video camera.

Photothermal Experiments. The near-infrared (NIR) LED (1 × 1 cm, 8.7 W, 845 nm) chip was applied as the NIR light source. YM was dispersed in deionized water and exposed to the NIR light irradiation for 400 s. The distance of the NIR LED chip from YM suspension surface was kept as 14 mm. To determine the photothermal effects of the YM/PU films, these films were irradiated under the NIR light for 50 s, while the distance of the NIR LED chip and the films were 10 mm. The temperature of the YM suspensions and YM/PU films were recorded with an FLIR thermal imaging camera and a Vernier Thermal Analysis Plus software. To measure the photothermal-induced shape memory properties of YM/PU film, the thin film (10 mm × 5 mm × 0.1 mm) was folded while the thick film (10 mm × 5 mm × 1 mm) was rolled, and the column was stretched to the diameter of ~2 mm at 90 °C, followed by putting them at room temperature and then irradiating under the NIR light. The distances between the NIR LED chip and the films were kept as 10 mm for thin film, and 12 mm for both thick film and column. The thermal response time was recorded by a Canon DSLR camera.

In Vitro Stability. The films (10 mm × 5 mm × 0.1 mm) were divided into three groups: (1) PU; (2) YM/PU-2 wt %; and (3) YM/PU-2 wt % after NIR light irradiation. The degree of film degradation was evaluated by determining the residual weight. Each group containing 36 samples were weighed and labeled as original weight (w_t). The *in vitro* degradation of each film was performed in the closed sample vial (20 mL) containing PBS solution (4 mL, 0.1 M, pH 7.4) as the degradation medium. The PBS solution was prepared using the Na₂HPO₄ and NaH₂PO₄·2H₂O, and the experiments were carried out in an incubator at 37 °C. During a period of 12 weeks, at the end of each week, three vials of the sample were taken, washed with ultrapure water, and dried in the oven at 50 °C for 48 h. The water absorption of the films were calculated based on the recording

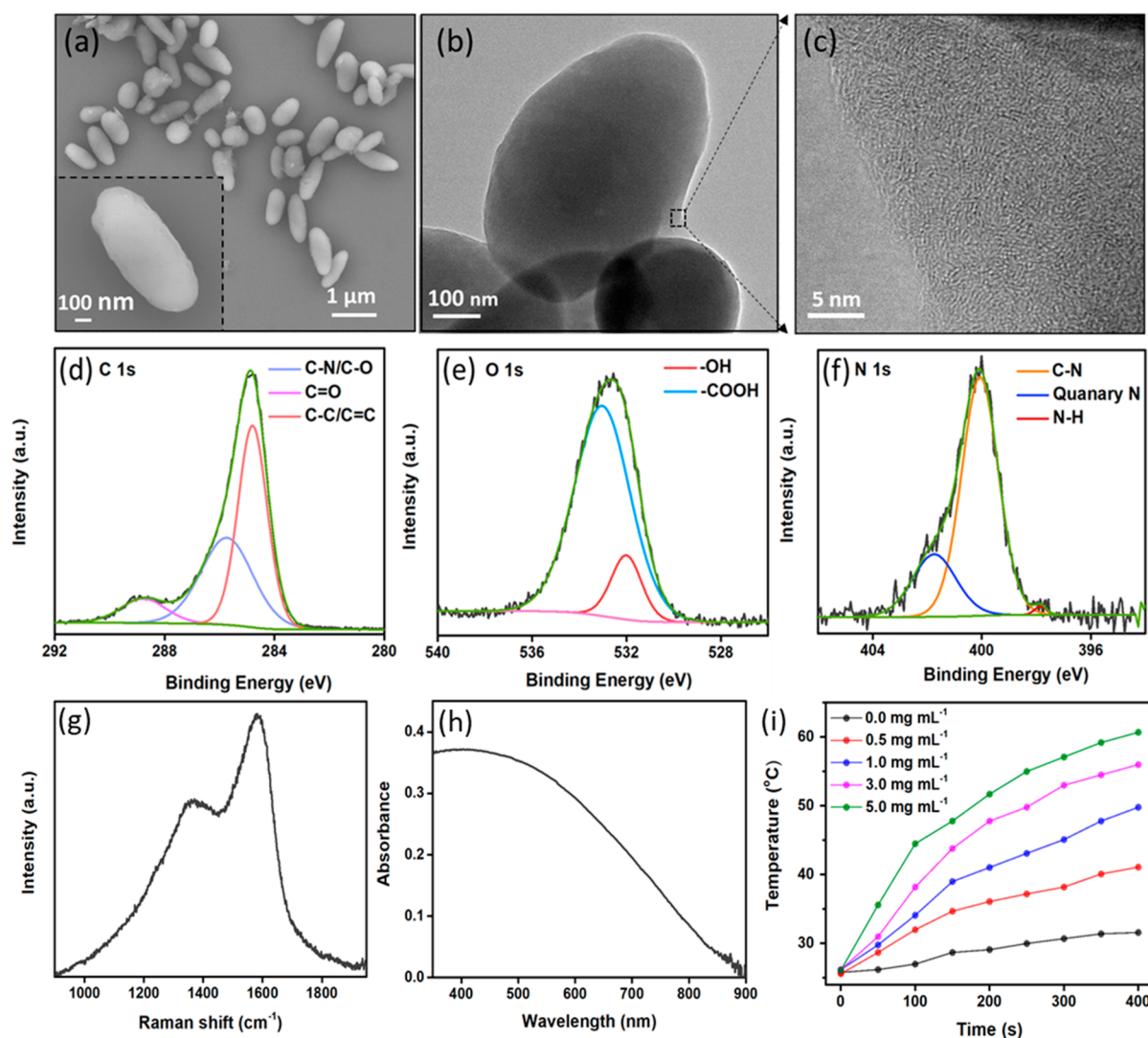


Figure 1. (a) SEM image of the YM particles. (inset) Single YM particle. (b) TEM image of the YM particles. (c) Enlarged area from panel b. High-resolution C 1s (d), O 1s (e), and N 1s (f) XPS from YM particles. (g) Raman spectra of YM particles. (h) UV-vis-NIR absorption spectra of YM particles dispersed in water. (i) Photothermal heating curves of the YM particles dispersed in water with different concentrations under NIR light irradiation.

data of the original weight (w_r) and weights before (w_a) and after (w_b) drying using the following eqs 1 and 2

$$\text{residual weight} = w_b/w_r \times 100\% \quad (1)$$

$$\text{water absorption} = (w_a - w_b)/w_b \times 100\% \quad (2)$$

In Vitro Cytotoxicity Assays. The prepared YM/PU films (YM: 0–2 wt %) were divided into two groups, before and after NIR light irradiations. The *in vitro* cytotoxicity of the YM/PU films were evaluated using the hMSCs and L929 cell lines according to the ISO 10993-5:2009 standard. The films (5 mm × 5 mm × 0.1 mm) were first disinfected by immersing in the 75% (v/v) ethanol for 30 min and washed with PBS (0.1 M, pH = 7.4) thrice prior to use. The hMSCs collection was approved by Monash Health HREC, and the approval number is 12387B. Typically, cells were maintained in H-DMEM (for hMSCs) or DMEM (for L929) medium supplemented with glutamax (2 mL, Gibco) and 10% fetal bovin serum (FBS) and incubated in a humidified atmosphere at 37 °C with 5% CO₂. For testing films, cells were seeded in a 96-well plate with 1×10^4 cells in 100 μ L of the cell culture medium and incubated overnight. Films were then added for a further incubation. The viable cells were indicated by the optical absorbance at 450 nm determined by a microplate spectrophotometer (GloMax Discover, Promega). The cell

viability was calculated by this formula: cell viability (%) = (mean of abs value of treatment group/mean abs value of control) × 100%. Cell morphology is performed using the light microscope and looking at the shape of the cells.

In Vivo Toxicity Examination. Twenty healthy female Balb/c mice (6 weeks old) (Charles Reiver Company) applied for the experiments and all the *in vivo* experiments were approved by the ethics committee of Jilin University. The mice were randomly divided into four groups with and without films as follows: (a) control; (b) PU; (c) YM-2 wt %/PU; and (d) YM-2 wt %/PU after NIR light irradiation. The films were implanted at the back subcutis of each mouse, followed by monitoring and comparing them with the control mice for 2 months. Blood panel analysis and serum biochemistry assay were conducted by collecting 0.8 mL blood from the mice after the mice are sacrificed. The major organs (kidney, lung, spleen, liver, and heart) were harvested, fixed in 10% neutral buffered formalin, processed into paraffin, sectioned at 5 mm, stained with hematoxylin and eosin, and examined by digital microscopy.

In Vivo Shape Memory Behavior. The Cy5.5 labeled YM/PU column (Cy5.5-YM/PU column) was first stretched to the diameter of ~ 2 mm at 90 °C and was then fixed at room temperature. The *in vivo* shape memory behavior was conducted by implanting a Cy5.5-YM/PU column (length ~ 9 mm, diameter ~ 2 mm) into the back

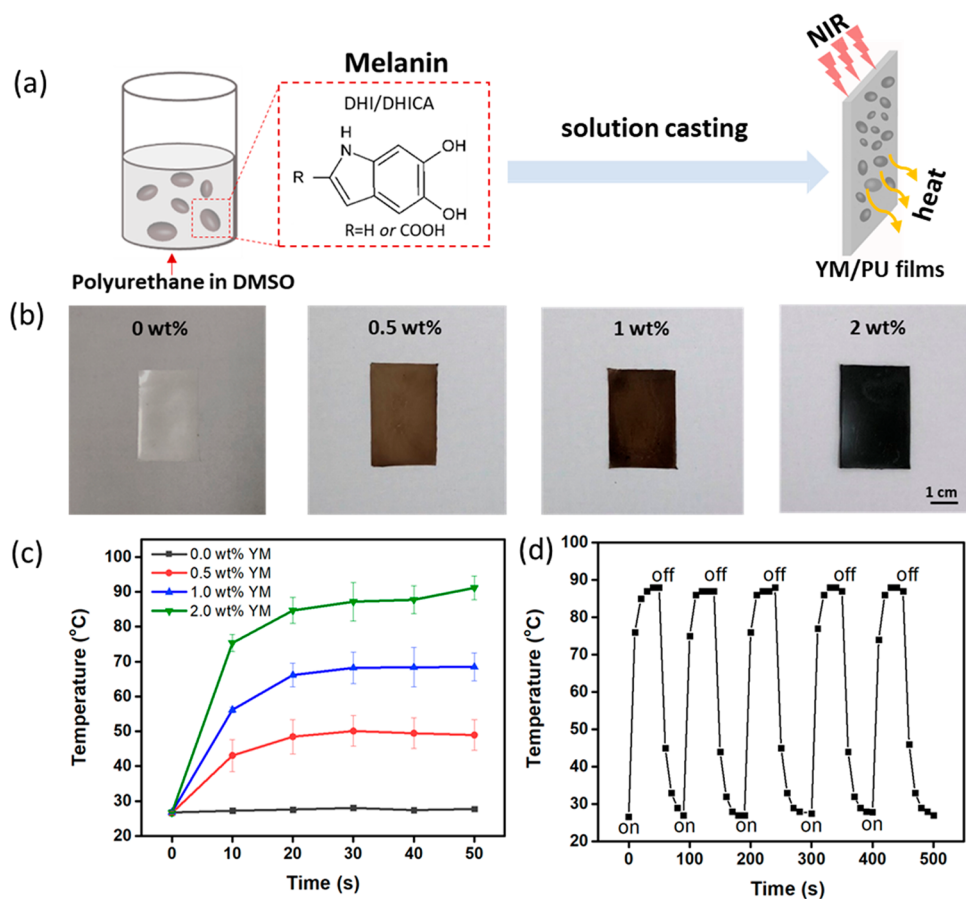


Figure 2. (a) Schematic illustration of preparation and working function of YM/PU films. (b) Photographs of the YM/PU films. (c) Photothermal heating curves of the YM/PU films with different YM contents irradiated by the 845 nm NIR LED chip. (d) Temperature elevation of YM/PU films with 2 wt % YM for five NIR LED on/off cycles.

subcutis and vagina of the female Balb/c nude mouse and exposed to an 808 nm laser. The shape memory behavior of the Cy5.5-YM/PU column was monitored by a fluorescence (Xenogen IVIS-Spectrum) imaging system. A peak wavelength of 673 nm was used as the excitation source and the Cy5.5 band-pass emission filter (707 nm) was conducted for 200 ms exposure time for each image frame.

RESULTS AND DISCUSSION

Preparation and Characterization of Yak Melanin. YM particles applied in this study were isolated from textile scrapes like yak hair wastes using the acidic isolation method. The isolated YM particles were characterized by SEM, TEM, HR-TEM, XPS, Raman spectroscopy, and UV-vis-NIR spectrophotometer as shown in Figure 1. It can be seen from Figure 1a,b that the YM are ellipsoidal particles. Our previous study have revealed that YM particles are eumelanin granules with longitudinal and traversal lengths of ~ 800 and ~ 400 nm, respectively.⁴³ Figure 1c reveals that YM particles are composed of nanoaggregations where curvature planes have been stacked through π - π stacking. This is consistent with the observations of *Sepia* melanin and bovine retinal epithelium melanin from Watt et al.⁴⁶ The structure of melanin revealed by their HR-TEM images is similar to those of partially disordered sp^2 carbon materials such as graphene and carbon black.⁴⁶ This similarity was further confirmed by the Raman spectra of the YM. As shown in Figure 1g, YM showed two strong Raman signals at 1360 and 1550 cm^{-1} , which were attributed to sp^2 carbon of 2D hexagonal structure lattice (D

band) and sp^2 carbon of in-plane aromatic structure ring (G band), respectively.^{13,47}

The planes in the nanoaggregation of YM are organized from the monomer of the melanin, including dihydroxyindole (DHI) and dihydroxyindole-carboxylic acid (DHICA).^{20,48} The functional groups in DHI and DHICA were disclosed by the XPS (Figure 1d-f) and FTIR (Figure S1) analyses of YM particles. Specifically, two peaks in the O 1s spectra locating at 532.003 and 533.027 eV represented the -OH and -COOH, respectively. The peaks in N 1s spectra were corresponding to the C-N (400.065 eV) and N-H (397.842 eV), while the peaks in C 1s spectra were in accordance with C-C/C=C (284.799 eV), C-N/C-O (285.732 eV), and C=O (288.779 eV) bonds, respectively.³² The prominent peak of quaternary N was not reported previously in the XPS analysis of the natural melanin.³² This peak might come from the residues from the yak hairs after the isolation process, since the same peak could be found in the human hair after heat treatment.⁴⁹ It might also arise from the strongly acidic treatment of indole units. Furthermore, in the FTIR spectra, the band positioning at around 3400 cm^{-1} raised from the O-H and N-H stretching,⁵⁰ while the band at around 1374 cm^{-1} was due to the -OH bending of the phenolic and carboxyl groups. The bending of the aromatic C=C and C=N also induced the band locating at around 1621 cm^{-1} .⁵¹

Due to the similar structural features between YM and sp^2 carbon materials, these two materials share some common optical properties, showing broadband and monotonic

absorption profile. As shown in the Figure 1h, YM has absorption from UV (350–400 nm) to visible (400–800 nm) and near-infrared (NIR) region (800–900 nm). The capability of the absorbing light in the NIR region promises the YM to be an excellent NIR photothermal agent. The suspensions containing different contents of YM were exposed to 845 nm NIR LED chip (8.7 W) to understand the photothermal effect (Figure 1i). It can be seen that the temperature increase of YM suspension (5 mg mL⁻¹) was 34.6 °C after NIR light irradiation for 400 s. In contrast, the temperature change of water was only by 5.8 °C, suggesting that YM particles converted NIR light into thermal energy effectively.

Preparation and Characterization of YM/PU Films. PU is composed of two segments including a hard segment determining the permanent shape, and a soft segment fixing the temporary shape below the shape memory transition temperature (T_{trans}). The phase separation between the hard and soft segments is responsible for the shape memory behavior of the PU.^{52,53} A “temporary” shape of PU can be obtained at a temperature higher than the T_{trans} and can be fixed by lowering the temperature below the T_{trans} . This “temporary” shape is able to recover to its “permanent” shape after increasing the temperature of PU over T_{trans} .⁴ To develop NIR-triggered SMPs, the YM was added into the PU and performed as the photothermal filler to increase the temperature over T_{trans} under NIR light irradiation, triggering the shape memory behavior of the PU. With increasing YM concentration, the YM/PU films had a darker color (Figure 2b) and showed higher absorption (Figure S2) in the NIR region, suggesting the successful incorporation of YM particles in the PU film. These YM/PU films also had very smooth surfaces without any observable clusters or agglomerates, indicating the homogeneous dispersion of YM particles in the PU. Furthermore, both PU and YM/PU films had similar water contact angles ($\sim 98^\circ$, Figure S3) and transition temperatures ($T_{trans} = \sim 65^\circ\text{C}$) (Figure S4). These results suggested that the incorporation of YM particles did not influence the surface energy of PU and did not change the T_{trans} of the PU.

The NIR photothermal performance of the YM/PU films with different YM concentrations was assessed by exposing the films to the NIR LED chip (845 nm, 8.7 W). As shown in Figure 2c, the temperature of pristine PU films did not change after the NIR light irradiation while the temperature of the YM/PU films increased as the YM concentration increased. Particularly, the temperature of the film with 1 wt % YM increased from 20 °C to $\sim 65^\circ\text{C}$ (T_{trans} of PU) after 50 s NIR light irradiation period. Furthermore, the YM-2 wt %/PU films were repeatedly irradiated with NIR lights for five times (Figure 2d), and it was observed that the photothermal effect of these films did not change, indicating their excellent photostability. It should be mentioned that the temperature decreased very quickly, which might be attributed to the fast heat transfer from melanin. It has been reported that the heat transfer time of the synthetic melanin with a diameter of 130 nm was around 1.7 ns,⁵⁴ and this might cause the observed drastic decrease of the temperature once the light source is turned off.

NIR-Photoresponsive Shape Memory Performance.

The shape memory performance of the YM/PU composites under NIR light irradiation was investigated. Two YM-2 wt %/PU films with different thicknesses were folded (10 mm \times 5 mm \times 0.1 mm) and rolled (10 mm \times 5 mm \times 1 mm),

respectively, at 90 °C and then cooled at room temperature for fixation to obtain temporary shapes. Figure 3a,b showed that

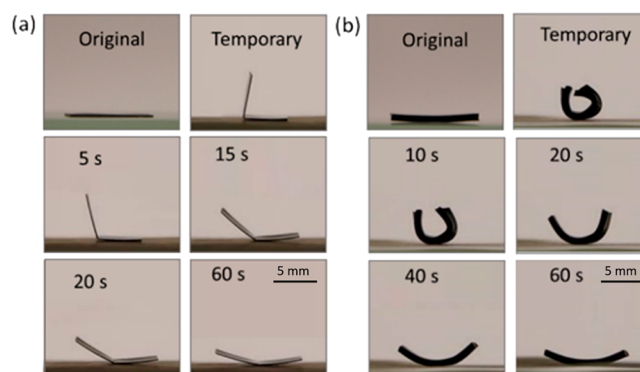


Figure 3. Photographs showing the NIR triggered shape memory behavior of a (a) folded thin YM-2 wt %/PU film and (b) rolled thick YM-2 wt %/PU film.

after NIR light irradiation, both YM-2 wt %/PU films gradually recovered to their original shapes. In contrast, the pristine PU film remained at its temporary shape (Figure S5). These results suggested that YM particles provided NIR photothermal performance and the addition of YM particles in the PU films played an important role in triggering their NIR-photoresponsive shape memory performance.

In Vitro Biocompatibility and Biostability. The viability of hMSCs and L929 cells was tested in the presence of YM/PU films with different YM contents, before and after NIR light irradiation, and was compared with untreated cells (Figure 4a,b). The viabilities of cells in the presence of YM/PU films with different YM content (0–2 wt %) were at around 80–90% after 24 h, indicating the low cytotoxicity of PU and YM/PU films to both hMSCs and L929 cells. Furthermore, the cell viability of YM/PU films before and after NIR light irradiation exhibited insignificant changes, suggesting that the NIR light irradiation did not induce additional cytotoxicity to the YM/PU films. Microscopic observation of cell size and morphology was carried out by phase contrast microscopy using L929 and hMSCs treated with films with different YM content (0–2 wt %) before and after NIR light irradiation (Figure S6). The cells did not change significantly from untreated cells within the exposure time further supporting lack of cell damage and cytotoxicity.

Mishra et al. conducted an *in vitro* hydrolytic study on the PU (Chronoflex-80A) for 12 months and found that the water uptake was $\sim 0.5\%$ and the molecular weight decrease was relatively modest.⁵⁵ The PU is thus considered as a good candidate to develop long-term implant devices due to its excellent *in vitro* biostability. It is important to understand if the added YM particles influence the *in vitro* biostability of the PU; therefore, the YM/PU films were immersed in the PBS (0.1 M, pH = 7.4) solution in an incubator (37 °C) for 12 weeks, during which the residue weight and water absorption of these films were recorded. As shown in Figure 4c, during these 12 weeks, the water absorption of pristine PU film remained at $\sim 1\%$, while the residue weight maintained at $\sim 99\%$. These findings are consistent with the results reported by the Mishra et al.⁵⁵ Most importantly, YM-2 wt %/PU films before or after NIR light irradiation had similar residual weight and water absorption values with those of the pristine PU. These results suggested that both YM addition and NIR light

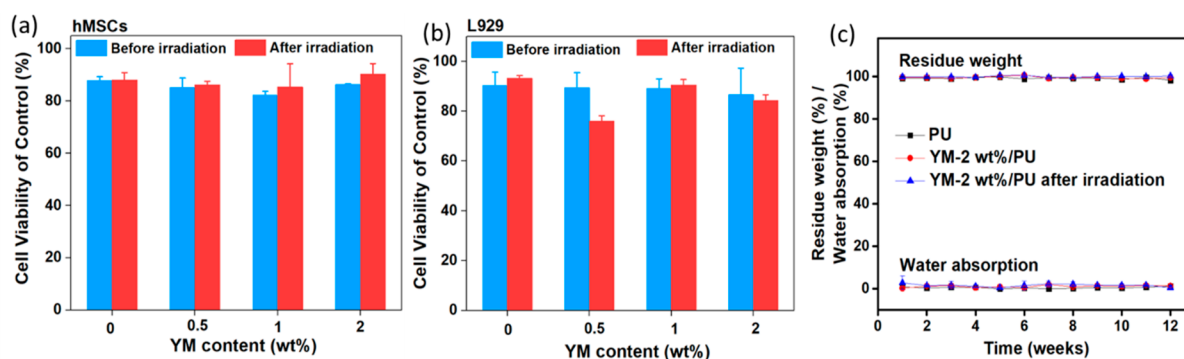


Figure 4. Cell viability of (a) hMSCs and (b) L929 after exposure to YM/PU films with different YM content for 24 h. (c) Water absorption and residue weight of the PU, YM-2 wt %/PU films, and YM-2 wt %/PU after NIR light irradiation in the PBS solution (0.1 M, pH = 7.4) at 37 °C for 12 weeks.

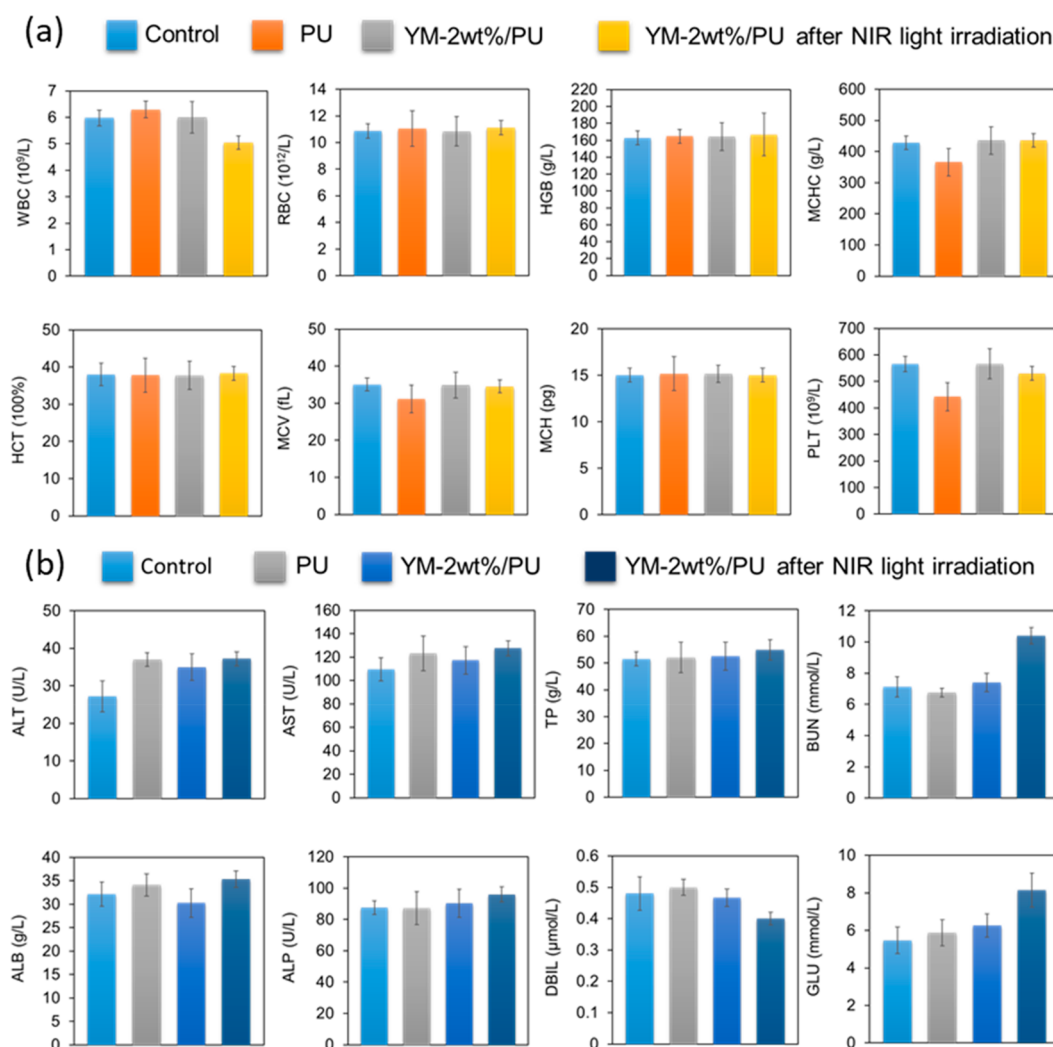


Figure 5. (a) Hematology analysis (WBC, RBC, HGB, MCHC, HCT, MCV, MCH and PLT). (b) Blood chemistry analysis (ALT, AST, TP, BUN, ALB, ALP, DBIL, GLU) of the mice after implantation of the PU, YM-2 wt %/PU, and YM-2 wt %/PU films with NIR light irradiation for 2 months. All analyses were compared with the mice without any treatment as a control.

irradiation did not influence the stability of the PU, and thus the YM/PU composites would be promising to develop as NIR photoresponsive implant materials.

In Vivo Toxicity. Twenty healthy female Balb/c mice were divided into four groups randomly, including the mice without any treatment (control), implanted with pristine PU film, YM-

2 wt %/PU film, and YM-2 wt %/PU film after NIR light irradiation. After the implantation for 2 months, hematological, biochemical, and histological analyses were conducted for each mouse. The hematological analysis contains the measurements for the white blood cells (WBC), red blood cells (RBC), hemoglobin (HGB), mean corpuscular hemoglobin concen-

tration (MCHC), hematocrit (HCT), mean corpuscular volume (MCV), mean corpuscular hemoglobin (MCH), and platelets (PLT). Figure 5a shows that the parameters from both PU and YM-2 wt %/PU groups were close to those from the control group, indicating that the YM-2 wt %/PU did not produce any toxic effects. The biochemical analysis included the examinations of the alanine transaminase (ALT), aspartate transaminase (AST), total protein (TP), blood urea nitrogen (BUN), albumin (ALB), alkaline phosphatase (ALP), direct bilirubin (DBIL), and glucose (GLU), and the results are shown in Figure 5b. These results further confirmed that the PU and YM-2 wt %/PU groups did not generate deleterious effects as the obtained levels from these groups were close to those from the control group. It can also be realized that the YM/PU composites did not cause hepatic and kidney toxicity because the ALT, AST, and ALP levels were relevant to the functions of kidney and liver of mice.⁴ Moreover, major organs including the heart, liver, spleen, lung, and kidney were collected and sliced for hematoxylin and eosin (H&E) staining for the histological examination. As shown in Figure 6,

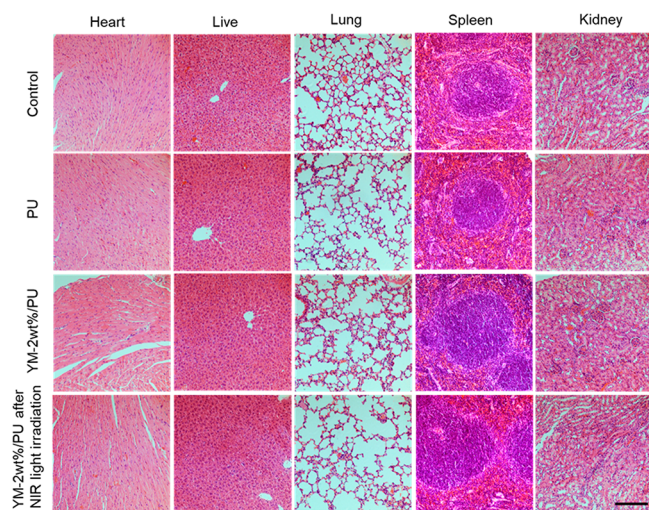


Figure 6. Histological result obtained from heart, liver, spleen, lung, and kidney after the implantation of PU, YM-2 wt %/PU, and YM-2 wt %/PU with NIR irradiation after two months (scale bars = 200 μm).

compared with the control group, no evident histopathological abnormalities or lesions were observed on the groups implanted with YM-2 wt %/PU composites (before and after NIR light irradiation), suggesting the good biocompatibility of the YM/PU composites.

In Vivo Shape Memory Behavior. The excellent NIR-triggered shape memory performance, biocompatibility, and biostability of the YM/PU composites suggested it as a potential long-term implant material. Here, we propose the application of the YM/PU column for the contraception as demonstrated in Figure 7a. Briefly, YM/PU column was prepared using a thermoplastic method and was stretched to a proper size that can be implanted the fallopian tube. Using the NIR light as the remote control, the YM/PU column was gradually recovered to its original size that was large enough to occlude the fallopian tube, thereby inhibiting the integration of sperm and egg to achieve contraception. *In vitro* shape memory recovery was demonstrated as shown in Figure 7b. By exposing the YM/PU column to the NIR LED chip (845 nm, 8.7 W),

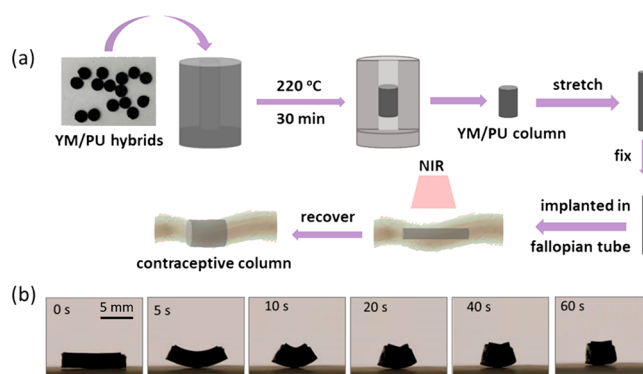


Figure 7. (a) Illustration scheme of the fabrication and working function of the contraception column based on the YM/PU composites. (b) *In vitro* recovery of the YM/PU column under the NIR light (845 nm).

the length of the column gradually changed from ~ 9 to ~ 4 mm, while its diameter changed from ~ 2 to ~ 3 mm.

To demonstrate *in vivo* shape memory behavior of the YM/PU column, a Cy5.5-labeled YM/PU column and an 808 nm laser were used. *In vitro*, the Cy5.5-labeled YM/PU column exhibited the similar recovery process to that under the 845 nm LED chip, indicating its successful shape memory behavior and potential to perform as contraception column (Figures 7b and 8a). The Cy5.5-labeled YM/PU column was implanted in

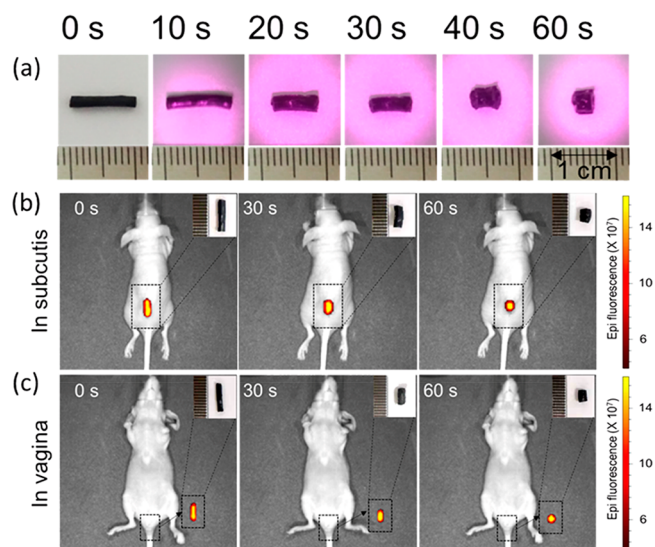


Figure 8. (a) Photographs showing the *in vitro* shape memory behavior of Cy5.5-labeled YM/PU column under the NIR laser. Fluorescence images and photographs showing the *in vivo* shape memory behavior of the Cy5.5-labeled YM/PU column in the (b) subcutis and (c) vagina of the mouse under the NIR laser. The NIR laser was 808 nm with an intensity of 0.5 W/cm².

the back subcutis of a female Balb/c nude mouse (Figure 8b), and its shape memory behavior was monitored by a fluorescence imaging system. It can be seen that, within 60 s, the stretched Cy5.5-labeled YM/PU column became shorter and thicker under the NIR laser (808 nm, 0.5 W/cm²), indicating an efficient shape recovery capability of the YM/PU column *in vivo*. Another Cy5.5-labeled YM/PU column was also implanted into the vagina of a mouse to simulate a fallopian tube. The Cy5.5 fluorescence cannot penetrate the

tissue because of the vagina was as deep as ~ 5 mm, and thus the column was taken out for fluorescence imaging every 30 s. Again, the shape memory behavior of the YM/PU column can be triggered by the NIR laser with an intensity of 0.5 W/cm^2 (Figure 8c). It is known that NIR light can penetrate the biological tissues with a depth of several centimeters;¹⁰ therefore, the NIR laser herein was able to trigger the recovery behavior of the YM/PU column. Additionally, the laser power intensity and exposure time applied in this study were comparable to the one used for the black phosphorus (BP)-based fallopian tube. The applied power intensity was also lower than those generally used for the photothermal therapy ($1\text{--}2 \text{ W/cm}^2$).^{4,13,34} These results demonstrated the practicability of our developed column, which was designed as the implant prototype based on the melanin for the first time. It should be mentioned that the mouse implanted with YM/PU column did not show any abnormalities after the *in vivo* recovery experiments, confirming the safety of the protocol.

CONCLUSIONS

In summary, the incorporation of YM to PU enabled a rapid temperature increase over the T_{trans} of the PU under the NIR light irradiation, thus triggering the shape memory behavior of the YM/PU composites. The *in vitro* and *in vivo* toxicity experiments firmly demonstrated the biocompatibility of the YM/PU composites. The *in vitro* degradation experiments also suggested that the YM/PU composites exhibited excellent biostability and, therefore, are promising “smart” implants by using the NIR light source as the remote control. The YM/PU composites could be easily reshaped through the thermoplastic method and their *in vivo* shape memory behavior was demonstrated by being implanted in the back subcutis and vagina of the mouse. In addition to their fabrication into a column that would be implanted in the fallopian tube for the purpose of contraception as proposed in this study, it could also be developed as other implantable devices such as self-expanding stents, active catheters, and so on. Given the abundance of natural melanin, easy availability of PU, and simple fabrication processing of the natural melanin/PU composites in any designed shapes, these natural melanin based-shape memory implants could be cost-effective materials in the biomedical industry.

ASSOCIATED CONTENT

Supporting Information

The Supporting Information is available free of charge at <https://pubs.acs.org/doi/10.1021/acsbomaterials.0c00933>.

FTIR spectra of yak melanin (Figure S1), UV–vis-NIR absorption spectra of YM/PU films with different YM content and absorbance values of YM/PU films at 845 nm (Figure S2), images of water contact angles on the PU and YM/PU films (Figure S3), DSC curve of pristine PU and YM-2 wt %/PU hybrids (Figure S4), photographs showing the pristine folded PU film ($10 \text{ mm} \times 5 \text{ mm} \times 0.1 \text{ mm}$) and rolled PU film ($10 \text{ mm} \times 5 \text{ mm} \times 1 \text{ mm}$) under NIR light irradiations for a certain period (Figure S5), and cell morphology of L292 and hMSCs after exposure to YM/PU film for 24 h (Figure S6) (PDF)

AUTHOR INFORMATION

Corresponding Authors

Lu Sun – Institute for Frontier Materials, Australian Future Fibers Research and Innovation Center, Deakin University, Geelong, Victoria 3220, Australia; orcid.org/0000-0003-2999-1250; Phone: +61 3 522 73247; Email: lu.sun@deakin.edu.au

Shi Zhan – State Key Laboratory of Inorganic Synthesis and Preparative Chemistry, International Joint Research Laboratory of Nano-Micro Architecture Chemistry (NMAC), International Research Center for Chemistry-Medicine Joint Innovation, College of Chemistry, Jilin University, Changchun 130012, China; orcid.org/0000-0001-9717-1487; Phone: +86 431 85168662; Email: zshi@mail.jlu.edu.cn

Authors

Wanjie Xie – Institute for Frontier Materials, Australian Future Fibers Research and Innovation Center, Deakin University, Geelong, Victoria 3220, Australia

Fei Yan – State Key Laboratory of Inorganic Synthesis and Preparative Chemistry, International Joint Research Laboratory of Nano-Micro Architecture Chemistry (NMAC), International Research Center for Chemistry-Medicine Joint Innovation, College of Chemistry, Jilin University, Changchun 130012, China; orcid.org/0000-0003-4750-1200

Esfandiar Pakdel – Institute for Frontier Materials, Australian Future Fibers Research and Innovation Center, Deakin University, Geelong, Victoria 3220, Australia

Julie Sharp – Institute for Frontier Materials, Australian Future Fibers Research and Innovation Center, Deakin University, Geelong, Victoria 3220, Australia

Dan Liu – Institute for Frontier Materials, Australian Future Fibers Research and Innovation Center, Deakin University, Geelong, Victoria 3220, Australia

Xungai Wang – Institute for Frontier Materials, Australian Future Fibers Research and Innovation Center, Deakin University, Geelong, Victoria 3220, Australia

Complete contact information is available at: <https://pubs.acs.org/doi/10.1021/acsbomaterials.0c00933>

Author Contributions

[§]These authors contributed equally to this work.

Notes

The authors declare no competing financial interest.

ACKNOWLEDGMENTS

This work was supported by the National Natural Science Foundation of China Nos. 81870117 and 21621001, the 111 Project No. B17020 and the Jilin Province Science and Technology Development Plan No. 20190201252JC. Dr. W. Xie would like to acknowledge the Australian Government Research Training Program Fees Offset Scholarship and Deakin University Postgraduate Research Scholarship. Deakin University's Advanced Characterization Facility is acknowledged for the use of the JEOL 2100F and the assistance from Rosey Squire.

REFERENCES

(1) Biswas, A.; Singh, A. P.; Rana, D.; Aswal, V. K.; Maiti, P. Biodegradable Toughened Nanohybrid Shape Memory Polymer for Smart Biomedical Applications. *Nanoscale* **2018**, *10* (21), 9917–9934.

- (2) Lendlein, A.; Behl, M.; Hiebl, B.; Wischke, C. Shape-Memory Polymers as a Technology Platform for Biomedical Applications. *Expert Rev. Med. Devices* **2010**, *7* (3), 357–379.
- (3) Xue, L.; Dai, S.; Li, Z. Biodegradable Shape-Memory Block Copolymers for Fast Self-Expandable Stents. *Biomaterials* **2010**, *31* (32), 8132–8140.
- (4) Xie, H.; Shao, J.; Ma, Y.; Wang, J.; Huang, H.; Yang, N.; Wang, H.; Ruan, C.; Luo, Y.; Wang, Q. Q.; Chu, P. K.; Yu, X. F. Biodegradable Near-Infrared-Photoresponsive Shape Memory Implants Based on Black Phosphorus Nanofillers. *Biomaterials* **2018**, *164*, 11–21.
- (5) Pang, X.; Xu, B.; Qing, X.; Wei, J.; Yu, Y. Photo-Induced Bending Behavior of Post-Crosslinked Liquid Crystalline Polymer/Polyurethane Blend Films. *Macromol. Rapid Commun.* **2018**, *39*, 1700237.
- (6) Zhang, Y.; Li, Y.; Liu, W. J. A. F. M. Dipole–Dipole and h-bonding Interactions Significantly Enhance the Multifaceted Mechanical Properties of Thermoresponsive Shape Memory Hydrogels. *Adv. Funct. Mater.* **2015**, *25* (3), 471–480.
- (7) Bai, Y.; Zhang, J.; Chen, X. A Thermal-, Water-, and Near-Infrared Light-Induced Shape Memory Composite Based on Polyvinyl Alcohol and Polyaniline Fibers. *ACS Appl. Mater. Interfaces* **2018**, *10* (16), 14017–14025.
- (8) Small, W.; Singhal, P.; Wilson, T. S.; Maitland, D. J. Biomedical Applications of Thermally Activated Shape Memory Polymers. *J. Mater. Chem.* **2010**, *20* (17), 3356–3366.
- (9) Zheng, N.; Fang, Z.; Zou, W.; Zhao, Q.; Xie, T. Thermoset Shape-Memory Polyurethane with Intrinsic Plasticity Enabled by Transcarbamoylation. *Angew. Chem., Int. Ed.* **2016**, *55*, 11421–11425.
- (10) Xu, R. X.; Povoski, S. P.; Martin, E. W., Jr. Targeted Delivery of Microbubbles and Nanobubbles for Image-Guided Thermal Ablation Therapy of Tumors. *Expert Rev. Med. Devices* **2010**, *7* (3), 303–306.
- (11) Xia, N.; Li, N.; Rao, W.; Yu, J.; Wu, Q.; Tan, L.; Li, H.; Gou, L.; Liang, P.; Li, L.; Meng, X. Multifunctional and Flexible ZrO₂-coated EGaIn Nanoparticles for Photothermal Therapy. *Nanoscale* **2019**, *11* (21), 10183–10189.
- (12) Zhang, X.; Chen, G.; Liu, Y.; Sun, L.; Sun, L.; Zhao, Y. Black Phosphorus-Loaded Separable Microneedles as Responsive Oxygen Delivery Carriers for Wound Healing. *ACS Nano* **2020**, *14* (5), 5901–5908.
- (13) Jiang, Q.; Luo, Z.; Men, Y.; Yang, P.; Peng, H.; Guo, R.; Tian, Y.; Pang, Z.; Yang, W. Red Blood Cell Membrane-Camouflaged Melanin Nanoparticles for Enhanced Photothermal Therapy. *Biomaterials* **2017**, *143*, 29–45.
- (14) Magrez, A.; Kasas, S.; Salicio, V.; Pasquier, N.; Seo, J. W.; Celio, M.; Catsicas, S.; Schwaller, B.; Forró, L. Cellular Toxicity of Carbon-Based Nanomaterials. *Nano Lett.* **2006**, *6* (6), 1121–1125.
- (15) Wu, M.-C.; Deokar, A. R.; Liao, J.-H.; Shih, P.-Y.; Ling, Y.-C. Graphene-Based Photothermal Agent for Rapid and Effective Killing of Bacteria. *ACS Nano* **2013**, *7* (2), 1281–1290.
- (16) Neelgund, G. M.; Oki, A. Advancement in Photothermal Effect of Carbon Nanotubes by Grafting of Poly (amidoamine) and Deposition of CdS Nanocrystallites. *Ind. Eng. Chem. Res.* **2018**, *57* (23), 7826–7833.
- (17) Zeng, J.; Shi, D.; Gu, Y.; Kaneko, T.; Zhang, L.; Zhang, H.; Kaneko, D.; Chen, M. J. B. Injectable and Near-Infrared-Responsive Hydrogels Encapsulating Dopamine-Stabilized Gold Nanorods with Long Photothermal Activity Controlled for Tumor Therapy. *Biomacromolecules* **2019**, *20* (9), 3375–3384.
- (18) Xie, W.; Pakdel, E.; Liang, Y.; Kim, Y. J.; Liu, D.; Sun, L.; Wang, X. Natural Eumelanin and Its Derivatives as Multifunctional Materials for Bio-inspired Applications: A Review. *Biomacromolecules* **2019**, *20* (12), 4312–4331.
- (19) Kumar, P.; Di Mauro, E.; Zhang, S.; Pezzella, A.; Soavi, F.; Santato, C.; Cicoira, F. Melanin-Based Flexible Supercapacitors. *J. Mater. Chem. C* **2016**, *4* (40), 9516–9525.
- (20) Kim, Y. J.; Wu, W.; Chun, S. E.; Whitacre, J. F.; Bettinger, C. J. Catechol-Mediated Reversible Binding of Multivalent Cations in Eumelanin Half-Cells. *Adv. Mater.* **2014**, *26* (38), 6572–6579.
- (21) Kim, Y. J.; Khetan, A.; Wu, W.; Chun, S. E.; Viswanathan, V.; Whitacre, J. F.; Bettinger, C. J. Evidence of Porphyrin-Like Structures in Natural Melanin Pigments Using Electrochemical Fingerprinting. *Adv. Mater.* **2016**, *28* (16), 3173–3180.
- (22) Tian, Z.; Hwang, W.; Kim, Y. J. Mechanistic Understanding of Monovalent Cation Transport in Eumelanin Pigments. *J. Mater. Chem. B* **2019**, *7*, 6355–6361.
- (23) Wang, Y.; Li, T.; Ma, P.; Bai, H.; Xie, Y.; Chen, M.; Dong, W. Simultaneous Enhancements of UV-shielding Properties and Photostability of Poly (vinyl alcohol) via Incorporation of Sepia Eumelanin. *ACS Sustainable Chem. Eng.* **2016**, *4* (4), 2252–2258.
- (24) Wang, Y.; Li, T.; Wang, X.; Ma, P.; Bai, H.; Dong, W.; Xie, Y.; Chen, M. Superior Performance of Polyurethane Based on Natural Melanin Nanoparticles. *Biomacromolecules* **2016**, *17* (11), 3782–3789.
- (25) Liang, Y.; Xie, W.; Pakdel, E.; Zhang, M.; Sun, L.; Wang, X. Homogeneous Melanin/Silica Core-Shell Particles Incorporated in Poly (methyl methacrylate) for Tunable UV Protection and Enhanced Thermal Stability. *Mater. Chem. Phys.* **2019**, *230*, 319–325.
- (26) Liang, Y.; Pakdel, E.; Zhang, M.; Sun, L.; Wang, X. Photoprotective Properties of Alpaca Fiber Melanin Reinforced by Rutile TiO₂ Nanoparticles: A Study on Wool Fabric. *Polym. Degrad. Stab.* **2019**, *160*, 80–88.
- (27) Wang, Z.; Zou, Y.; Li, Y.; Cheng, Y. Metal-Containing Polydopamine Nanomaterials: Catalysis, Energy, and Theranostics. *Small* **2020**, *16* (18), No. 1907042.
- (28) Yang, P.; Zhang, S.; Chen, X.; Liu, X.; Wang, Z.; Li, Y. Recent Developments in Polydopamine Fluorescent Nanomaterials. *Mater. Horiz.* **2020**, *7* (3), 746–761.
- (29) Yang, P.; Gu, Z.; Zhu, F.; Li, Y. Structural and Functional Tailoring of Melanin-Like Polydopamine Radical Scavengers. *CCS Chemistry* **2020**, *2* (2), 128–138.
- (30) Manini, P.; Panzella, L.; Eidenberger, T.; Giarra, A.; Cerruti, P.; Trifuoggi, M.; Napolitano, A. Efficient Binding of Heavy Metals by Black Sesame Pigment: Toward Innovative Dietary Strategies To Prevent Bioaccumulation. *J. Agric. Food Chem.* **2016**, *64* (4), 890–7.
- (31) Sen, T.; Barrow, C. J.; Deshmukh, S. K. Microbial Pigments in the Food Industry—Challenges and the Way Forward. *Front. Nutr.* **2019**, *6*, 7.
- (32) Kim, Y. J.; Wu, W.; Chun, S.-E.; Whitacre, J. F.; Bettinger, C. J. Biologically Derived Melanin Electrodes in Aqueous Sodium-Ion Energy Storage Devices. *Proc. Natl. Acad. Sci. U. S. A.* **2013**, *110* (52), 20912–20917.
- (33) Meredith, P.; Sarna, T. The Physical and Chemical Properties of Eumelanin. *Pigm. Cell Res.* **2006**, *19* (6), 572–94.
- (34) Kim, M.; Kim, H. S.; Kim, M. A.; Ryu, H.; Jeong, H. J.; Lee, C. M. Thermohydrogel Containing Melanin for Photothermal Cancer Therapy. *Macromol. Biosci.* **2017**, *17* (5), 1600371.
- (35) Fan, Q.; Cheng, K.; Hu, X.; Ma, X.; Zhang, R.; Yang, M.; Lu, X.; Xing, L.; Huang, W.; Gambhir, S. S.; Cheng, Z. Transferring Biomarker Into Molecular Probe: Melanin Nanoparticle as a Naturally Active Platform for Multimodality Imaging. *J. Am. Chem. Soc.* **2014**, *136* (43), 15185–15194.
- (36) Liu, Y.; Ai, K.; Liu, J.; Deng, M.; He, Y.; Lu, L. Dopamine-Melanin Colloidal Nanospheres: An Efficient Near-Infrared Photothermal Therapeutic Agent for In Vivo Cancer Therapy. *Adv. Mater.* **2013**, *25* (9), 1353–1359.
- (37) Li, Z.; Yang, Y.; Wang, Z.; Zhang, X.; Chen, Q.; Qian, X.; Liu, N.; Wei, Y.; Ji, Y. Polydopamine Nanoparticles Doped in Liquid Crystal Elastomers for Producing Dynamic 3D Structures. *J. Mater. Chem. A* **2017**, *5* (14), 6740–6746.
- (38) Yang, L.; Wang, Z.; Fei, G.; Xia, H. Polydopamine Particles Reinforced Poly(vinyl alcohol) Hydrogel with NIR Light Triggered Shape Memory and Self-Healing Capability. *Macromol. Rapid Commun.* **2017**, *38*, 1700421.
- (39) Tian, H.; Wang, Z.; Chen, Y.; Shao, J.; Gao, T.; Cai, S. Polydopamine-Coated Main-Chain Liquid Crystal Elastomer as Optically Driven Artificial Muscle. *ACS Appl. Mater. Interfaces* **2018**, *10* (9), 8307–8316.

(40) Li, Z.; Zhang, X.; Wang, S.; Yang, Y.; Qin, B.; Wang, K.; Xie, T.; Wei, Y.; Ji, Y. Polydopamine Coated Shape Memory Polymer: Enabling Light Triggered Shape Recovery, Light Controlled Shape Reprogramming and Surface Functionalization. *Chem. Sci.* **2016**, *7* (7), 4741–4747.

(41) Yang, L.; Tong, R.; Wang, Z.; Xia, H. Polydopamine Particle-Filled Shape-Memory Polyurethane Composites with Fast Near-Infrared Light Responsibility. *ChemPhysChem* **2018**, *19* (16), 2052–2057.

(42) Liang, Y.; Han, Q.; Byrne, N.; Sun, L.; Wang, X. Recyclable One-Step Extraction and Characterization of Intact Melanin from Alpaca Fibers. *Fibers Polym.* **2018**, *19* (8), 1640–1646.

(43) Xie, W.; Pakdel, E.; Liu, D.; Sun, L.; Wang, X. Waste-Hair-Derived Natural Melanin/TiO₂ Hybrids as Highly Efficient and Stable UV-Shielding Fillers for Polyurethane Films. *ACS Sustainable Chem. Eng.* **2020**, *8* (3), 1343–1352.

(44) Xie, W.; Pakdel, E.; Liang, Y.; Liu, D.; Sun, L.; Wang, X. Natural Melanin/TiO₂ Hybrids for Simultaneous Removal of Dyes and Heavy Metal Ions under Visible Light. *J. Photochem. Photobiol., A* **2020**, *389*, 112292.

(45) Horvath, A. L. Solubility of Structurally Complicated Materials: 3. Hair. *Sci. World J.* **2009**, *9*, 255–271.

(46) Watt, A. A. R.; Bothma, J. P.; Meredith, P. The Supramolecular Structure of Melanin. *Soft Matter* **2009**, *5* (19), 3754–3760.

(47) Galvan, I.; Jorge, A.; Ito, K.; Tabuchi, K.; Solano, F.; Wakamatsu, K. Raman Spectroscopy as a Non-Invasive Technique for The Quantification of Melanins in Feathers and Hairs. *Pigm. Cell Melanoma Res.* **2013**, *26* (6), 917–923.

(48) Meredith, P.; Powell, B. J.; Riesz, J.; Nighswander-Rempel, S. P.; Pederson, M. R.; Moore, E. G. Towards Structure–Property–Function Relationships for Eumelanin. *Soft Matter* **2006**, *2* (1), 37–44.

(49) Zhao, Z.-Q.; Xiao, P.-W.; Zhao, L.; Liu, Y.; Han, B.-H. Human Hair-Derived Nitrogen and Sulfur Co-Doped Porous Carbon Materials for Gas Adsorption. *RSC Adv.* **2015**, *5* (90), 73980–73988.

(50) Wang, Y.; Wang, X.; Li, T.; Ma, P.; Zhang, S.; Du, M.; Dong, W.; Xie, Y.; Chen, M. Effects of Melanin on Optical Behavior of Polymer: From Natural Pigment to Materials Applications. *ACS Appl. Mater. Interfaces* **2018**, *10* (15), 13100–13106.

(51) Mboniyirivuze, A.; Mwakikunga, B.; Dhlamini, S. M.; Maaza, M. Fourier Transform Infrared Spectroscopy for Sepia Melanin. *Phys. Mater. Chem.* **2015**, *3* (2), 25–29.

(52) Liu, W.; Zhao, Y.; Wang, R.; Li, J.; Li, J.; Luo, F.; Tan, H.; Fu, Q. Post-Crosslinked Polyurethanes with Excellent Shape Memory Property. *Macromol. Rapid Commun.* **2017**, *38*, 1700450.

(53) Zhao, Q.; Qi, H. J.; Xie, T. Recent Progress in Shape Memory Polymer: New Behavior, Enabling Materials, and Mechanistic Understanding. *Prog. Polym. Sci.* **2015**, *49–50*, 79–120.

(54) Ju, K. Y.; Kang, J.; Pyo, J.; Lim, J.; Chang, J. H.; Lee, J. K. pH-Induced Aggregated Melanin Nanoparticles for Photoacoustic Signal Amplification. *Nanoscale* **2016**, *8* (30), 14448–14456.

(55) Mishra, A.; Seethamraju, K.; Delaney, J.; Willoughby, P.; Faust, R. Long-Term In Vitro Hydrolytic Stability of Thermoplastic Polyurethanes. *J. Biomed. Mater. Res., Part A* **2015**, *103* (12), 3798–3806.